Improved CO_2 photocatalytic reduction using a novel 3-component heterojunction

Teera Butburee[†1,2], Zhuxing Sun[†3,4], Anthony Centeno[5,6], Fang Xie[5], Zhefei Zhao[7], Daxiong Wu[8], Piangjai Peerakiatkhajohn[1], Supphasin Thaweesak[1], Haiqiang Wang*[3] and Lianzhou Wang*[1]

[1]Nanomaterials Centre, School of Chemical Engineering and Australian Institute for Bioengineering and Nanotechnology, the University of Queensland, St Lucia, QLD, 4072, Australia

[2]National Nanotechnology Center, National Science and Technology Development Agency, 111 Thailand Science Park, Pathum Thani 12120, Thailand

[3]Key Laboratory of Environment Remediation and Ecological Health, Ministry of Education, College of Environmental & Resources Science, Zhejiang University, Hangzhou 310058, P.R. China

[4]School of Environmental Science and Engineering, Shanghai Jiao Tong University, Shanghai 200240, China

[5]Department of Materials and London Centre for Nanotechnology, Imperial College London, London, UK

[6]Department of Electrical and Electronic Engineering, Xi'an Jiaotong Liverpool University, Jiangsu 215123, China

[7]School of Mechanical and Energy Engineering, Zhejiang University of Science and Technology, Hangzhou 310023, PR China

[8]College of Materials Science and Engineering, Qingdao University of Science and Technology, Qingdao, China

[†]These authors contribute to this work equally

*Corresponding Author, Email: l.wang@uq.edu.au; haiqiangwang@zju.edu.cn

Abstract

A new class of three-component photocatalyst system is designed with plasmonic AuCu nanoprisms embedded between a porous single crystalline TiO_2 nanoplate thin film and dodecahedral zeolitic imidazolate frameworks (ZIF-8) nanoparticles for enhanced CO_2 photocatalytic reduction. The ZIF-8 plays a role of CO_2 capture to enhance the reactant concentration on the catalyst, while the AuCu nanoprism functions as an important mediator to improve the charge density at the interfaces and facilitate the charge transfer from TiO_2 to ZIF-8. The reactant CO_2 could be not only readily collected on the newly designed catalyst, but also more efficiently converted to CO and CH_4. As a result, compared to the reference sample of two-component system of TiO_2 and ZIF-8 with a CO_2 conversion rate of 12.5 μmol $h^{-1}{\cdot}g^{-1}$, the new three-component photocatalyst exhibited a nearly 7-fold improvement in CO_2 photocatalytic reduction performance with CO_2 conversion reaching an outstanding value of86.9 μmol $h^{-1}{\cdot}g^{-1}$, highlighting the importance of rational heterojunction design in facilitating reactant adsorption, charge transfer and reaction processes in photocatalysis.

Introduction

To alleviate the green-house effect and worldwide energy shortage, carbon dioxide (CO_2) photocatalytic reduction, which aims to utilize sunlight to convert the greenhouse gases into valuable chemicals, is both fundamentally and technologically fascinating.[1, 2] Since the early trials by Halmann[3], Hemminger[4] and Inoue[5] et al. in the 1970s, numerous semiconductor photocatalysts and their derivatives have been explored for CO_2 photocatalytic reduction.[2, 6, 7] However, very few of the reported catalysts achieve a conversion exceeding tens of micromole per gram of catalysts per hour when irradiated by simulated sunlight.[2, 8-10] Two of the major issues leading to low CO_2 reduction efficiencies are the fast recombination of photo-generated electron-hole pairs in and on the semiconductor and the low affinity of CO_2 on the catalysts with limited active sites.[11-15] To facilitate the separation and transportation of the photo-excited charge carriers on the catalysts, various strategies have been developed including facet and morphology engineering,[16-19] heterojunction construction,[20-22] and deposition of noble metal nanoparticles[23-25]. However, approaches to increase the CO_2 concentration on the catalysts' surface for timely consumption of the separated charges were relatively less explored.[26]

Recently, photocatalysts with enhanced CO_2 adsorption have been attempted by integrating semiconductor photocatalysts with metal-organic frameworks (MOFs) which have excellent capability in capturing gas molecules.[27-32] For instance, by growing one type of zeolitic imidazolate frameworks, ZIF-8, on Zn_2GeO_4 nanorods 3.8-time enhancement in CO_2 adsorption can be achieved.[27] Li et al.[28] aeheys er n heeedyed e de iseh nys MOFs [$Cu_3(BTC)_2$] core to capture CO_2 and macro-porous TiO_2 shells for photoexcitation and confirmed electron transfer from TiO_2 to $Cu_3(BTC)_2$. A zirconium metal-organic framework, UiO-66, with strong CO_2 capture ability was incorporated with graphitic carbon nitride (g-C_3N_4).[29] However, despite the greatly improved CO_2 uptake, the overall product yield for CO_2 photocatalytic reduction on these catalysts showed moderate increase (1.6-3.4 times), suggesting that only a small ratio of the adsorbed CO_2 was converted to desirable chemicals during the photocatalytic process. How to

make better use of the captured CO_2 on these photocatalysts enhance the CO_2 reduction efficiency remains a challenge.

Herein, we present a new strategy to facilitate the CO_2 conversion in the photocatalyst systems by deliberately introducing plasmonic nanoparticles in between the CO_2 adsorbent and the semiconductor. Our idea was to selectively deposit the plasmonic nanoparticles at the interface of two key components, ie. photocatalyst and CO_2 adsorber which could act as both an amplifier for photo-excited charges and a transfer bridge. As a proof of this concept, a three-component structure was constructed by a simple two-step procedure with a 2D mesoporous single-crystalline TiO_2 (denoted as 2DT) vertically grown on FTO glass as the semiconductor base (Figure S1-2); ZIF-8 [$Zn(MeIm)_2$, MeIm = 2-methylimidazolate] with high thermal stability and excellent CO_2 capturing ability[33-36] as the CO_2 adsorbent and AuCu triangular nanoprisms as the plasmonic particles.[37] Encouragingly, extraordinarily enhanced CO_2 reduction efficiency, 21 and 8 times that of commercial TiO_2 (P25) and pristine 2DT, respectively, was realized on this specifically designed heterojunction structure under simulated sunlight, due to the synergistic effect of ZIF-8 and plasmonic nanoparticles in facilitating CO_2 adsorption and charge transfer.

Results and Discussion

Figure 1a schematically illustrates the construction procedure for the three-component junction of TiO_2, AuCu, and ZIF-8. Firstly, the unique TiO_2 (2DT) films were obtained *in situ* on FTO glass via a hydrothermal and ion exchange route.[38] Subsequently, pre-synthesized AuCu nanoprisms with a side length of ~130 nm and a thickness of ~10 nm were spin-coated onto 2DT films. The samples obtained after this step are denoted as A-2DT. Then, single crystalline ZIF-8 was grown *in situ* on the top of A-2DT, resulting the formation of 2DT-AuCu-ZIF-8 3-component junctions. The sample is so assigned hereafter as 3J-2DT (See methods section for detailed procedures). It should be noted that the growth of ZIF-8 particles was random, without a selectivity. Therefore, besides the 3-component junctions, there were also bare ZIF-8 and AuCu on 2DT. The amount of AuCu loaded and the size of ZIF-8 were controlled by the number of cycles of spin coating and the concentration of synthesis precursors of ZIF-8, respectively. After optimization, the loading amount of AuCu was determined to be ~1.5 wt% based on Energy-dispersive X-ray Spectroscopy (EDS), and the size of ZIF-8 was 150~300 nm (Supporting Information). For comparison, a similar composite consisting of the same three components as 3J-2D (TiO_2, AuCu, and ZIF-8) but with AuCu and ZIF-8 all located separately on 2DT was also prepared. The fabrication procedure is schematically shown in Figure 1b. ZIF-8 was grown on 2DT first (denoted as Z-2DT) before the AuCu particles were spin-coated on the surface. Thus no AuCu particles could be embedded at the interface of 2DT and ZIF-8. All junctions formed consisted of only two components ZIF-8 and 2DT or AuCu and 2DT and so the sample was denoted as 2J-2DT.

The morphologies of the resultant 2J-2DT and 3J-2DT observed by scanning electron microscopy (SEM) are shown in Figures 1c and 1d. For both samples, ZIF-8 nanoparticles in dodecahedron structure are successfully grown on 2DT with an intimate contact. Note that while

AuCu particles always appear outside the junctions of 2DT and ZIF-8 on 2J-2DT, some AuCu nanoprisms were found embedded in between 2DT-ZIF-8 contact on 3J-2DT, forming the three-component junction. This was clearly observed by transmission electron microscopy (TEM) (Figure 1e). Energy-dispersive X-ray spectroscopy (EDS) mapping of 3J-2DT (Figure 1f) verified Ti and O in the 2D nanoplates, Au and Cu in the triangular nanoparticles (the signal of Cu is interfered by Cu signal from TEM copper grid) and metal element Zn in the dodecahedron, respectively. Furthermore, XPS spectra reveal that the major peak of Cu $2p^{3/2}$ at 932.7 eV and a weak satellite at ~943 eV (Figure S4), indicating the presence of Cu mainly in metallic state with trace amount on the surface oxidized to CuO/Cu_2O.[37] The X-ray powder diffraction (XRD) patterns of 2J-2DT and 3J-2DT (Figure 1g) were almost identical, indicating that both samples have the same compositions. Compared to the XRD pattern of 2DT, it was revealed that the 2D titanium material was in anatase phase which was maintained after decoration of ZIF-8 and AuCu. Diffraction peaks of ZIF-8 can be clearly observed on the XRD pattern for both 2J-2DT and 3J-2DT. However, no peak related to Au, Cu or their alloys in the XRD pattern of 3J-2DT was observed, probably due to the low content of the metal nanoprisms (1.5 wt%).

Figure 2a shows the UV-Visible light absorption spectra of bare 2DT, composite of 2DT and ZIF-8 (Z-2DT), 2DT decorated by AuCu particles (A-2DT), 2J-2DT and 3J-2DT. Pure 2DT has a light absorption band only in UV region. When only ZIF-8 was grown on this 2DT, slight change in the light absorption spectra was observed. In contrast, A-2DT with AuCu deposited 2DT presented a wide and broad absorption band in the visible light range with a maxima at ~580 nm. The UV-vis absorption spectra of 2J-2DT and 3J-2DT were similar to each other. In particular, wideband absorption induced by AuCu nanoprisms was observed in both cases. However, the absorption intensity was decreased to a certain extent for both samples which could be attributed to increased reflection of the incident light by ZIF-8. [39, 40]

To better understand the visible-light absorption peak of the smaples, calculations using the Finite Difference Time Domain (FDTD) technique were carried out (see supporting information for a full description). Note that FDTD calculations for AuCu were not considered reliable because of the lack of a suitable Drude-Lorentz model. Therefore, the adsorption of Au and Cu nanoprism were simulated, respectively. In particular, it was found that the visible adsorption observed was attributed to the local surface plasma resonance (LSPR) effect of the side facets of the nanoprisms, which were with a height of ~10 nm, rather than the triangle surfaces.[41] This is considered reasonable because the TiO_2 nanoplates grew vertically on the FTO glass, forming a dense film, while the AuCu nanoprisms lay flat on the surface of the nanoplates. Therefore, when the light irradiated the top of the film in the experiments, the AuCu nanoprisms fronted the light mainly by their side planes. Figure 2b shows the absorption spectra for Au and Cu nanoprisms with the incident light from one side and the corresponding electric field enhancement on the triangular surface under the irradiation of 520 nm light (inset). The enhanced electric field is a direct reflection of the increased photo-excited charges at the 3-component interfaces. In addition, it was also beneficial for promoting electron transfer from the metal to ZIF-8.

Nitrogen (N_2) adsorption-desorption isotherms of the as-prepared samples (Fig. 2c) reveal that the surface areas of the composite materials (2J-2DT and 3J-2DT) were greatly improved by the deposition of ZIF-8 (978.6 $m^{2}\cdot g^{-1}$). While the original 2DT had a total surface area of around 107.3 $m^{2}\cdot g^{-1}$, the specific surface areas of 2J-2DT and 3J-2DT were 487.3$m^{2}\cdot g^{-1}$ and 461.4 $m^{2}\cdot g^{-1}$, respectively. With this ~4-time improvement in surface areas, the CO_2 adsorptions on 2J-2DT and 3J-2DT could be significantly enhanced.[26, 27, 34, 42] Meanwhile, the similar surface areas of 2J-2DT and 3J-2DT imply that the two sample should also possess similar CO_2 adsorption capacity.

The two composites with an identical composition but different structures (2J-2DT and 3J-2DT) were tested in CO_2 photocatalytic reduction under simulated sunlight irradiation. For comparison, the performances of commercial TiO_2 (P25), 2DT, Z-2DT, and A-2DT are also presented (Figure 2d). The productions of CO and CH_4 from this P25 film were 3.5 and 0.6 $\mu mol\cdot h^{-1}\cdot g^{-1}$, respectively. Owing to the excellent intrinsic properties of 2DT,[38] CO and CH_4 yields of 9.1 $\mu mol\cdot h^{-1}\cdot g^{-1}$ and 1.8 $\mu mol\cdot h^{-1}\cdot g^{-1}$ respectively were obtained on pure 2DT, both were about 3 times larger than P25. However, this production was still very limited. When ZIF-8 was grown on 2DT (2DT-Z), the CO_2 production only increased from 10.9 to 12.61 $\mu mol\cdot h^{-1}\cdot g^{-1}$. This suggests that although ZIF-8 significantly improved the gas adsorption ability of the catalyst, it did not significantly enhance the overall CO_2 reduction efficiency, possibly due to the limited electron density and transfer rate between the two components (2DT and ZIF-8).[43] This could also be inferred from the fact that the ratio of CH_4, which require 8 electrons to produce in contrast to the two-electron reaction to CO, in the final products was dramatically decreased with Z-2DT (from 16.1% for 2DT to 2.0%).

Considering A-2DT, a greater enhancement in activity was found with a product yield of 24.4 $\mu mol\cdot h^{-1}\cdot g^{-1}$, suggesting the much stronger promotion effect of AuCu nanoprism (which enhanced the light absorption and electron transportation) compared to ZIF-8. The CO_2 reduction rate achieved on 2J-2DT was around 36.7 $\mu mol\cdot h^{-1}\cdot g^{-1}$, which is nearly the sum of the productions on Z-2DT and A-2DT. However, when some of the AuCu nanoprisms were embedded between ZIF-8 and TiO_2 (i.e. 3J-2DT), the total production reached as high as 86.9 $\mu mol\cdot h^{-1}\cdot g^{-1}$, nearly 8 times that of pure 2DT and more than 21 times that of P25. This verifies the importance of three-component heterojunctions with AuCu embedded between 2DT and ZIF-8.

The time-course evolution of CO and CH_4 from CO_2 on 2J-2DT and 3J-2DT are presented in Figure 3a. The linear increase in the productions with time indicate the stability of both samples in CO_2 photocatalytic reduction. The superiority of the 3-component system can be clearly observed, with more than double the yields of both products. Because the light absorption and CO_2 adsorption ability for both 3-component samples were similar to each other, the major contribution to better CO_2 reduction performance on sample 3J-2DT should be attributed to in the special structured 3-component junction, where the adsorbed high-density CO_2 in ZIF-8 could encounter the high-density excited charges from the AuCu-TiO_2 interface, thus leading to a more efficient CO_2 conversion.

Life-time spectra of photo-generated charges on 2J-2DT and 3J-2DT were obtained using time-resolved photoluminescence with 377 nm exciton (Figure 3b). The lifetime of photo-excited charges in 3J-2DT was found to be longer than that of the 2J-2DT, which could be attributed to the more fluent charge transfer routes (TiO_2→AuCu→ZIF-8) of the 3-component junctions. In this light, a larger amount of photo-induced electron-hole pairs on 3J-2DT were participating in the redox reaction.

Based on the above observation and discussion, a working mechanism for the enhanced CO_2 photocatalytic performance on 3J-2DT is proposed, as schematically illustrated in Figure 3c. When AuCu and ZIF-8 are separately dispersed on 2DT, the charge density at the interface and the transfer of charges between 2DT and ZIF-8 are limited. When a three-component junction is constructed with AuCu nanoprism in between the ZIF-8 dodecahedron and the 2DT plate, the plasmonic nanoparticles not only act as a charge transportation bridge between ZIF-8 and TiO_2[44] but also locally enhance the electromagnetic field[45-47]. The AuCu nanoprisms with their 2D feature allow them to have excellent contact on 2DT plates. Moreover, this Janus-like structure can be of advantageous for its excellent anisotropic charge separation. [48, 49] This allows a fluent collection of photo-excited charges from 2DT by AuCu. In addition, hot-electron transfer under visible light excitation leads to a greatly enhanced electron density in vicinal areas where ZIF-8 is present. Accordingly, more concentrated electrons could be accessed by the CO_2 adsorbed on the ZIF-8 and are subsequently reduced with protons.

Conclusion

In conclusion, we demonstrated a new strategy of rational heterojunction structure design to promote the in-situ photoreduction of adsorbed CO_2 in semiconductor-absorbent photocatalyst systems. By introducing plasmonic nanoparticles, AuCu nanoprisms between 2D porous single crystalline TiO_2 (2DT) and ZIF-8, forming a 3-component photocatalyst (3J-2DT), the photocatalytic activity for CO_2 reduction in the presence of water vapor increased by 7 times compared to the 2-component one with only ZIF-8 and 2DT (Z-2DT). The AuCu nanoprisms played two essential roles in this system. They allowed the catalyst to have an extended wide absorption band in visible light range, which led to locally enhanced electromagnetic field with enriched photo-excited charges at the interfaces. Also, the metal nanoparticles acted as a medium to facilitate the charge transfer between the semiconductor and the CO_2 adsorbent. The new strategy presented herein not only provides an effective way to design better photocatalyst systems, but also would inspire for the design of advanced catalysts that could have the features of reaction absorption and in-situ reaction in other applications.

Experimental

Synthesis

Synthesis of 2DT: 2DT was synthesized according to the method we reported recently.[38] Briefly, 0.438 g of potassium titanium oxalate was dissolved in 3 mL of water under mechanical

stirring for 15 minutes. Then, 37 mL of diethylene glycol was added and further stirred for 15 minutes. The mixture was transferred to a 250 mL Teflon-lined autoclave which contain an 3x3 cm^2 FTO substrate (FTO side was down against the autoclave wall, the angle was ~20-25°). The reactor was heated up to 180 °C for 9 hours. The film was rinsed with ethanol after the reactor was cooled down, and dried in a vacuum oven set at 70 °C for 12 hours. The film was then calcined at 400 °C for 2 hours iseh ramping rate rf 2 $°C \cdot min^{-1}$. After cooled down to room temperature, the film was ion-exchanged by soaking in 0.04 M aqueous HCl, for 3 hours (HCl solution was refreshed every hour). Then, the film was rinsed with a pious amount of DI water, dried in a vacuum oven set at 70 °C for 12 hours, and calcined in the identical process as the first calcinations.

Synthesis of AuCu nanoprisms: AuCu nanoprisms were synthesized according to the reported method with slight modification.[37] Firstly, Triangular Au template were synthesized by seed-mediated method, with multiplication to have the total growth solution of 1 L. After collected, and purified, triangular Au particles were centrifuged and diluted in 20 mL of water. Then, 20 mL of 10 mM tetrabuthylammonium borohydride was added to the Au nanoparticle suspension with mechanical stirring. To this solution, 20 mL of 4 mM copper acetate was then added drop-wise over the course of 5 minutes. The resultant nanoparticles were therefore become Au decorated by Cu nanoparticles[37]. The suspension was allowed to rest for 30 minutes before centrifugation and rinse the top aliquot out to dispose the exceed borohydride. The particles were re-dispersed in 10 mL of the mixture of 1:1 water:methanol for further use.

2DT-Z synthesis: The epitaxial growth of ZIF-8 was performed by modifying the method developed by Lu et al. [50] Briefly, the 3x3 cm^3 TiO_2 film on FTO substrate was soaked in 1 $mg \cdot mL^{-1}$ aqueous solution of polyvinylpyroridone (PVP, Mw=55,000) for 24 hours to modify the surface suitable for ZIF-8 deposition. After blow dried, the film was soaked in the mixture of 20:20 mL of methanolic $Zn(NO_3)_2$ (12.5 mM) and methanolic 2-methylimmidazol (12.5 mM). The reaction was allowed for 24 hours. Then, the film was rinsed by copious amount of methanol before drying in the vacuum oven set at 70 °C for 12 hours.

2DT-A synthesis: AuCu nanoprism suspension was spin coated on 2DT film with the speed of 500 rpm for 30 seconds. The ratio of AuCu loading can be controlled by the number of coating cycles. It was found that 20 cycles of coating shown the best performance (the elemental ratio can be found in Supporting Information S5).

2J-2DT synthesis: First, ZIF-8 was grown on 2DT in the same way as 2DT-Z synthesis. Then, AuCu suspension was spin-coated for 20 cycles.

3J-2DT synthesis: First, AuCu was deposited on 2DT for 20 cycles (in the same way as 2DT-A synthesis). Then, the film was soaked in PVP solution to modify the surface, and grew ZIF-8 in the same way as synthesizing 2DT-Z.

Synthesis of P25 film: The P25 film was prepared by dipping the suspension of P25 powder (~4.3 mg) onto a FTO glass (the same size of 2DT sample) and dried naturally.

The mass of catalysts were determined by weighting the glass substrate before and after synthesis. The exact mass = (weight the substrate after the synthesis) - (weight the substrate before the synthesis)

Characterization

Field emission scanning electron microscopy (JEOL JSM-7100F) operated at 10-20 kV was used for observing the morphologies of the composites. HRTEM, SAED, EDS mapping and elemental analysis were performed on JEOL 2100F Transmission electron microscope (200 kV). Crystallographic details were analysed by X-ray Diffraction (XRD) on a Bruker Advanced X-ray Diffractometer (40 kV, 30 mA) with Cu Kα radiation. UV-Vis light absorption properties were measured by Shimadzu 2200 UV-vis spectrophotometer.

CO_2 photocatalytic reduction test

Photocatalytic reduction of CO_2 was carried out in a batch reactor made of glass with a quartz window on the top. Typically, the 3×3 cm^2 film sample on FTO glass and 20 ml deionized water was placed respectively in the middle and at the bottom of the reactor, as shown in Fig.1. The reactor was vacuumed and filled with pure CO_2 (99.999%) for 3 times before it was set to ambient pressure and irradiated with 1.5 AM simulated sunlight from a Xe lamp (Newport 67005, USA). During the test, the temperature of the reactor was kept at 25 °C by a water bath. In each hour, 0.3 mL of gas was extracted with a syringe and injected into an Agilent 7890A GC for testing CO, CH_4 and other hydrocarbons. All ehe ymmpley i ede eeyee frd 3 esmey nar ehe mena vnl ey i edepdeyeaeer sa ehe ndes le

Acknowledgement

The authors acknowledge the financial support from Australian Research Council (Discovery Projects), National Nanotechnology Center (NANOTEC, Thailand), Royal Thai Government Scholarship for Science and Technology, National Natural Science Foundation of China (No. 51578488 and No. 2180050404) and Program for Zhejiang Leading Team of S&T Innovation (Grant No. 2013TD07). AC acknowledges support from the XJTLU research development fund (RDF-17-01-12).

Conflict of Interest

The authors declare no conflict of interest.

Associated Content

Supporting Information can be obtained from the publisher or the corresponding author.

Reference

[1] S.N. Habisreutinger, L. Schmidt- Mende, J.K. Stolarczyk, Angew. Chem. Int. Ed., 52 (2013) 7372-7408.
[2] K. Li, B.S. Peng, T.Y. Peng, ACS Catal., 6 (2016) 7485-7527.

[3] M. Halmann, Nature, 275 (1978) 115-116.
[4] J.C. Hemminger, R. Carr, G.A. Somorjai, Chem. Phys. Lett., 57 (1978) 100-104.
[5] T. Inoue, A. Fujishima, S. Konishi, K. Honda, Nature, 277 (1979) 637-638.
[6] S.N. Habisreutinger, L. Schmidt-Mende, J.K. Stolarczyk, Angew. Chem. Int. Ed., 52 (2013) 7372-7408.
[7] S. Navalón, A. Dhakshinamoorthy, M. Álvaro, H. Garcia, ChemSusChem 6 (2013) 562-577.
[8] Q. Kang, T. Wang, P. Li, L. Liu, K. Chang, M. Li, J. Ye, Angew. Chem. Int. Ed., 127 (2015) 855-859.
[9] J. Hou, S. Cao, Y. Wu, F. Liang, L. Ye, Z. Lin, L. Sun, Nano Energy, 30 (2016) 59-68.
[10] M. Li, L. Zhang, M. Wu, Y. Du, X. Fan, M. Wang, L. Zhang, Q. Kong, J. Shi, Nano Energy, 19 (2016) 145-155.
[11] Z. Sun, S. Wang, Q. Li, M. Lyu, T. Butburee, B. Luo, H. Wang, J.M.T.A. Fischer, C. Zhang, Z. Wu, L. Wang, Adv. Sustain. Sys., 1 (2017) 1700003.
[12] W. Tu, Y. Zhou, Z. Zou, Adv. Mater., 26 (2014) 4607-4626.
[13] J.L. White, M.F. Baruch, J.E. Pander Iii, Y. Hu, I.C. Fortmeyer, J.E. Park, T. Zhang, K. Liao, J. Gu, Y. Yan, T.W. Shaw, E. Abelev, A.B. Bocarsly, Chem. Rev. , 115 (2015) 12888-12935.
[14] S. Xie, Q. Zhang, G. Liu, Y. Wang, Chem. Commun., 52 (2016) 35-59.
[15] P. Akhter, M.A. Farkhondehfal, S. Hernández, M. Hussain, A. Fina, G. Saracco, A.U. Khan, N. Russo, J. Environ. Chem. Eng., 4 (2016) 3934-3953.
[16] J. Yu, J. Low, W. Xiao, P. Zhou, M. Jaroniec, J. Am. Chem. Soc., 136 (2014) 8839-8842.
[17] J. Mao, L. Ye, K. Li, X. Zhang, J. Liu, T. Peng, L. Zan, Appl. Catal. B, 144 (2014) 855-862.
[18] W. Zhang, Y. Hu, L. Ma, G. Zhu, P. Zhao, X. Xue, R. Chen, S. Yang, J. Ma, J. Liu, Nano Energy, 53 (2018) 808-816.
[19] S. Qamar, F. Lei, L. Liang, S. Gao, K. Liu, Y. Sun, W. Ni, Y. Xie, Nano Energy, 26 (2016) 692-698.
[20] J. Jin, J. Yu, D. Guo, C. Cui, W. Ho, Small, 11 (2015) 5262-5271.
[21] D.K. Mishra, H.J. Lee, J. Kim, H.-S. Lee, J.K. Cho, Y.-W. Suh, Y. Yi, Y.J. Kim, Green Chem., 19 (2017) 1619-1623.
[22] F. Li, L. Zhang, J. Tong, Y. Liu, S. Xu, Y. Cao, S. Cao, Nano Energy, 27 (2016) 320-329.
[23] W.-N. Wang, W.-J. An, B. Ramalingam, S. Mukherjee, D.M. Niedzwiedzki, S. Gangopadhyay, P. Biswas, J. Am. Chem. Soc., 134 (2012) 11276-11281.
[24] M. Tahir, B. Tahir, N.A.S. Amin, Appl. Catal. B, 204 (2017) 548-560.
2 t e a u, A ac i -Agull , Concepci n , H. Garcia, J. Am. Chem. Soc., 136 (2014) 15969-15976.
[26] E. Pipelzadeh, V. Rudolph, G. Hanson, C. Noble, L. Wang, Appl. Catal. B, 218 (2017) 672-678.
[27] Q. Liu, Z.-X. Low, L. Li, A. Razmjou, K. Wang, J. Yao, H. Wang, J. Mater. Chem. A, 1 (2013) 11563-11569.
[28] R. Li, J. Hu, M. Deng, H. Wang, X. Wang, Y. Hu, H.L. Jiang, J. Jiang, Q. Zhang, Y. Xie, Adv. Mater., 26 (2014) 4783-4788.
[29] L. Shi, T. Wang, H. Zhang, K. Chang, J. Ye, Adv. Funct. Mater., 25 (2015) 5360-5367.
[30] Y. Zeng, R. Zou, Y. Zhao, Adv. Mater., 28 (2016) 2855-2873.
[31] S. Yan, S. Ouyang, H. Xu, M. Zhao, X. Zhang, J. Ye, J. Mater. Chem. A, 4 (2016) 15126-15133.
[32] M. Wang, D. Wang, Z. Li, Appl. Catal. B, 183 (2016) 47-52.

[33] K.S. Park, Z. Ni, A.P. Côté, J.Y. Choi, R. Huang, F.J. Uribe-Romo, H.K. Chae, M. O'Keeffe, O Yaghi, Proc. Natl. Acad. Sci., 103 (2006) 10186-10191.
[34] Y. Hu, Z. Liu, J. Xu, Y. Huang, Y. Song, J. Am. Chem. Soc., 135 (2013) 9287-9290.
[35] A. Phan, C.J. Doonan, F.J. Uribe-Romo, C B Knobler, O'keeffe, O Yaghi, Acc Chem. Res., 43 (2010) 58-67.
[36] K. Sumida, D.L. Rogow, J.A. Mason, T.M. McDonald, E.D. Bloch, Z.R. Herm, T.-H. Bae, J.R. Long, Chem. Rev., 112 (2012) 724-781.
[37] P.J. Straney, C.M. Andolina, J.E. Millstone, Isr. J. Chem. , 56 (2016) 257-261.
[38] T. Butburee, Y. Bai, H. Wang, H. Chen, Z. Wang, G. Liu, J. Zou, P. Khemthong, G.Q.M. Lu, L. Wang, Adv. Mater., 30 (2018) e1705666.
[39] T. Butburee, Y. Bai, J. Pan, X. Zong, C. Sun, G. Liu, L. Wang, J. Mater. Chem. A, 2 (2014) 12776-12784.
[40] S. Eslava, L. Zhang, S. Esconjauregui, J. Yang, K. Vanstreels, M.R. Baklanov, E. Saiz, Chem. Mater., 25 (2012) 27-33.
[41] Z. Chen, H. Dai, J. Liu, H. Xu, Z. Li, Z.-K. Zhou, J.-B. Han, Opt. Express, 21 (2013) 17568-17575.
[42] C.-H. Kuo, Y. Tang, L.-Y. Chou, B.T. Sneed, C.N. Brodsky, Z. Zhao, C.-K. Tsung, J. Am. Chem. Soc., 134 (2012) 14345-14348.
[43] G. Xu, H. Zhang, J. Wei, H.-X. Zhang, X. Wu, Y. Li, C. Li, J. Zhang, J. Ye, ACS Nano, 12 (2018) 5333-5340.
[44] H. Tada, T. Mitsui, T. Kiyonaga, T. Akita, K. Tanaka, Nat. Mater., 5 (2006) 782.
[45] J. Nelayah, M. Kociak, O. Stéphan, F.J.G. de Abajo, M. Tencé, L. Henrard, D. Taverna, I. Pastoriza-Santos, L.M. Liz-Marzán, C. Colliex, Nat. Phys., 3 (2007) 348.
[46] X.-b. Xu, Z. Yi, X.-b. Li, Y.-y. Wang, J.-p. Liu, J.-s. Luo, B.-c. Luo, Y.-g. Yi, Y.-j. Tang, J. Phys. Chem. C, 117 (2013) 17748-17756.
[47] J. Nelayah, M. Kociak, O. Stephan, N. Geuquet, L. Henrard, F.J. García de Abajo, I. Pastoriza-Santos, L.M. Liz-Marzán, C. Colliex, Nano Lett., 10 (2010) 902-907.
[48] Z.W. Seh, S. Liu, M. Low, S.Y. Zhang, Z. Liu, A. Mlayah, M.Y. Han, Adv. Mater., 24 (2012) 2310-2314.
[49] Z.W. Seh, S. Liu, S.Y. Zhang, M. Bharathi, H. Ramanarayan, M. Low, K.W. Shah, Y.W. Zhang, M.Y. Han, Angew. Chem., 123 (2011) 10322-10325.
[50] G. Lu, S. Li, Z. Guo, O.K. Farha, B.G. Hauser, X. Qi, Y. Wang, X. Wang, S. Han, X. Liu, J.S. DuChene, H. Zhang, Q. Zhang, X. Chen, J. Ma, S.C.J. Loo, W.D. Wei, Y. Yang, J.T. Hupp, F. Huo, Nat. Chem., 4 (2012) 310.

Figure

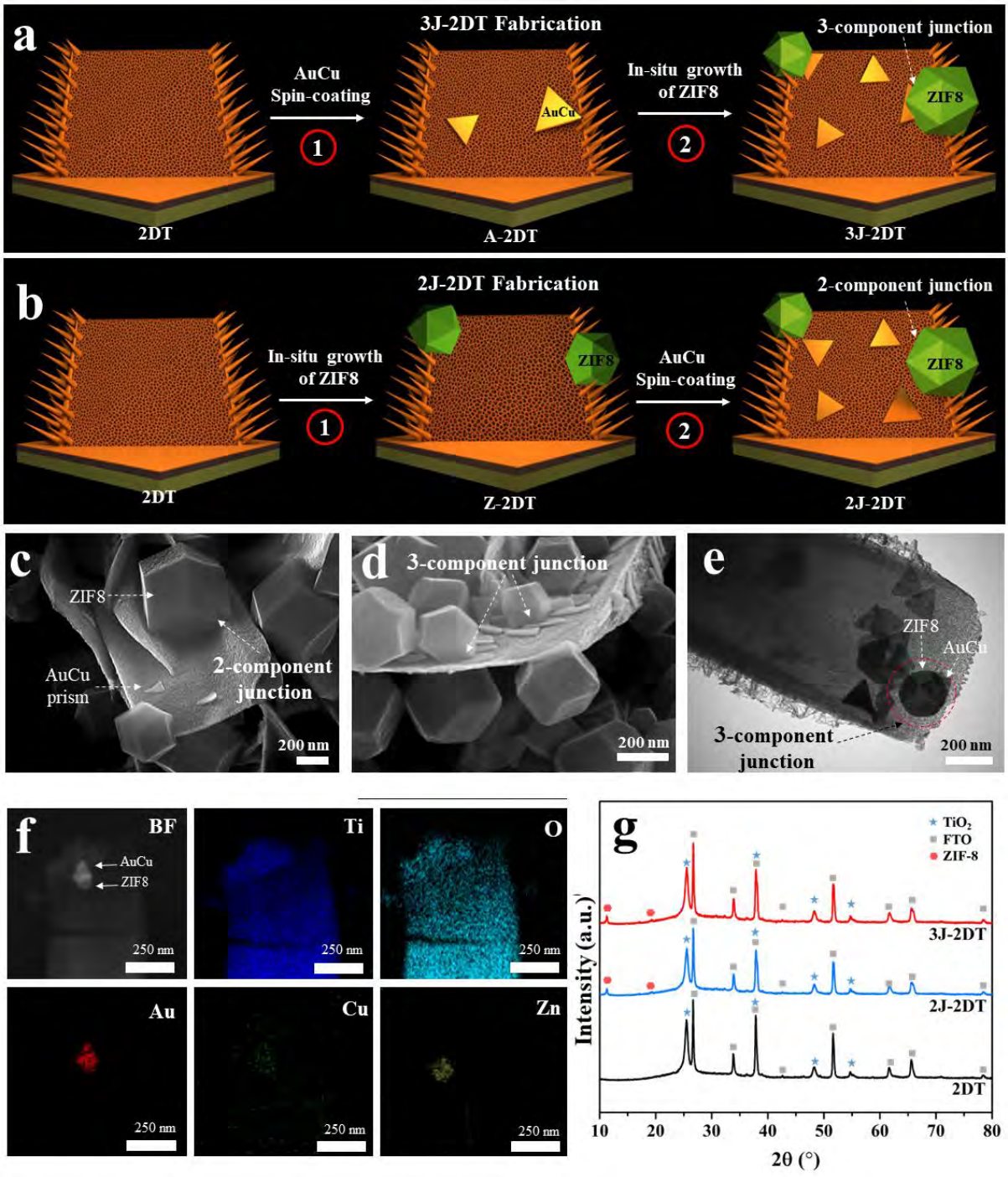

Figure 1 Fabrication Procedure of (a) 3J-2DT and (b) 2J-2DT; Typical SEM images of (c) 2J-2DT and (d) 3J-2DT; (e) TEM image of 3J-2DT; (f) Elemental distribution obtained from EDS mapping; (g) XRD patterns of 2DT, 2J-2DT and 3J-2DT.

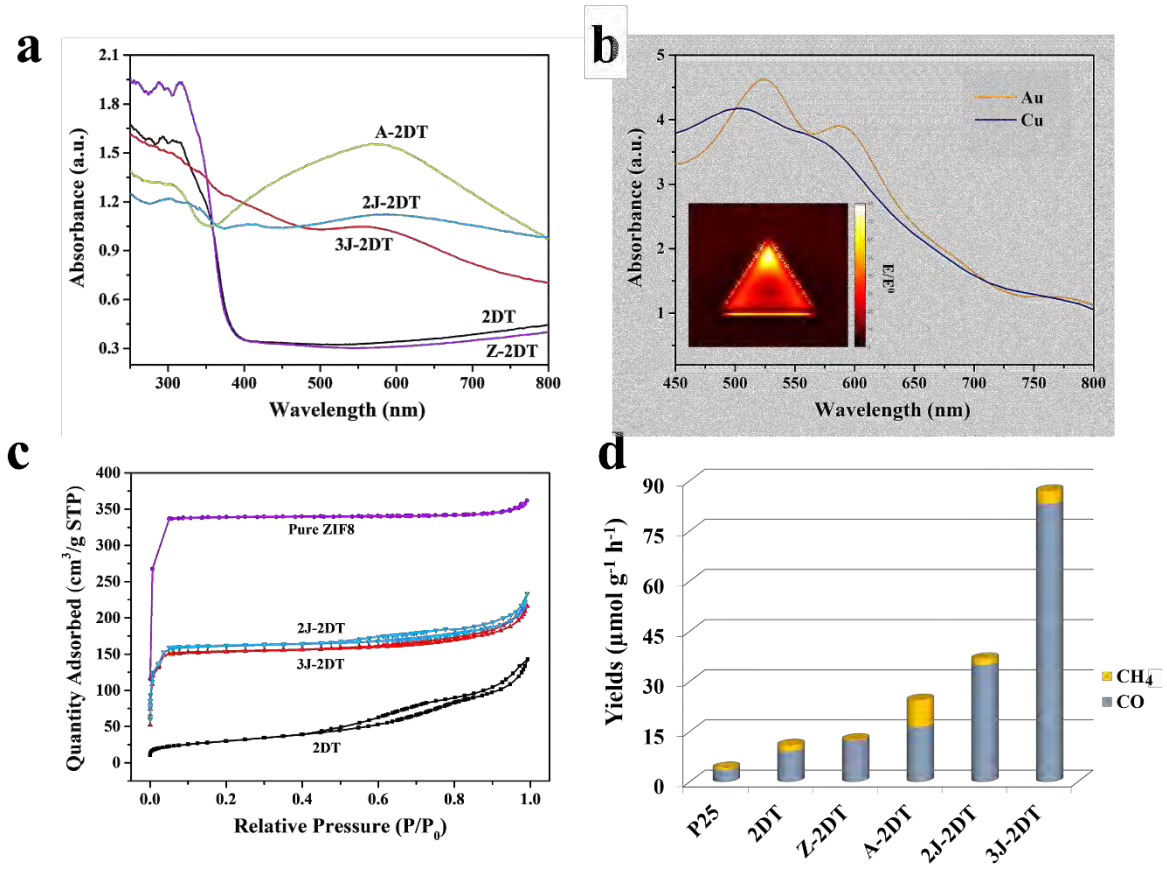

Figure 2 (a) UV-vis DRS spectra of various samples tested; (b) FDTD calculated absorption efficiency for Au and Cu nanoprism (The insert shows electric field enhancement at 520 nm at the interface between Au and ZIF-8); (c) N_2 adsorption-desorption curves of 2DT, 2J-2DT, 3J-2DT and pure ZIF-8; (d) Production of CO and CH_4 in CO_2 photocatalytic reduction on various samples.

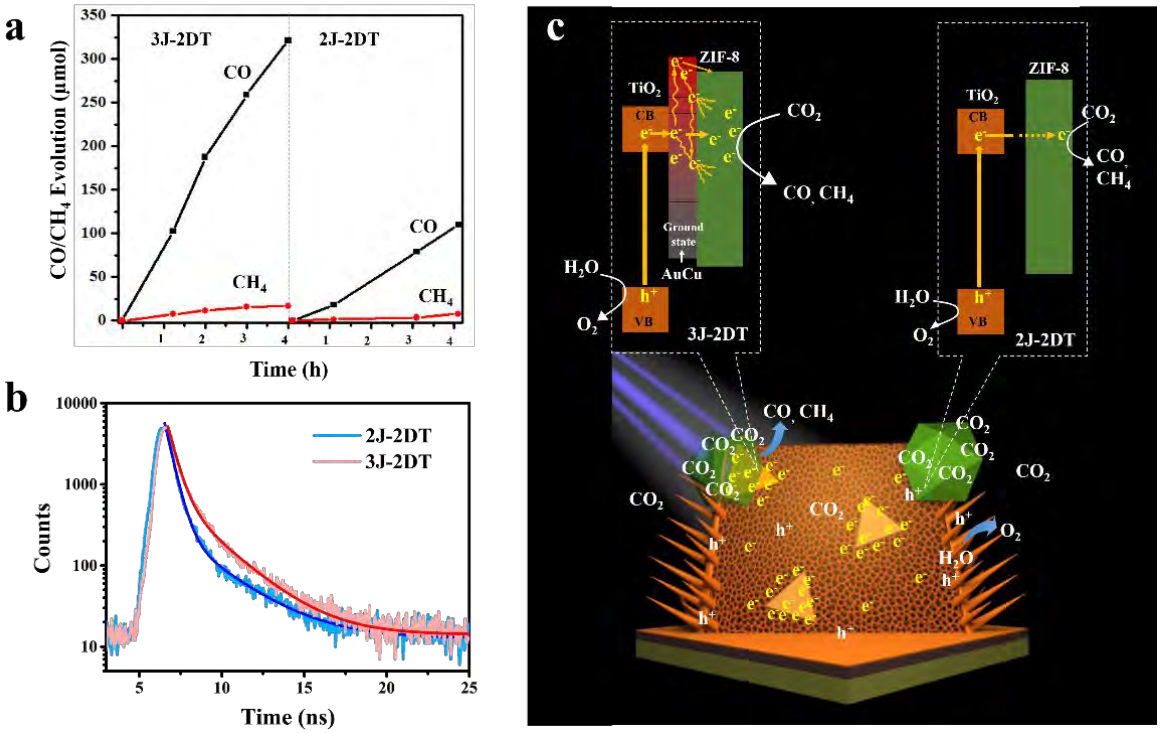

Figure 3 (a) Time-course productions of CO and CH_4 in CO_2 photocatalytic reduction on 3J-2DT and 2J-2DT. (b) Lifetime spectra of photo-generated charges on 2J-2DT and 3J-2DT with an excitation light of 377 nm; (c) Schematic illustration of the promoting mechanism of 3J-2DT compared to 2J-2DT

Supporting Information

Click here to download Supporting Information: Supporting Information.docx

Graphical Abstract